Transactions of Tianjin University (2023) 29:482–491
https://doi.org/10.1007/s12209-023-00377-8

RESEARCH ARTICLE

The Preparation of Nanosized Pd/ZSM-23 Bifunctional Catalysts for *n*-Hexadecane Hydroisomerization by Employing PHMB as the Growth Modifier

Jiazheng Sun[1] · Shuxiang Xiong[1] · Qiong Wu[1] · Wei Wang[1] · Wei Wu[1]

Received: 7 October 2023 / Revised: 23 October 2023 / Accepted: 13 November 2023 / Published online: 17 December 2023

Abstract
The development of highly effective metal–zeolite bifunctional catalysts for the hydroisomerization of *n*-alkanes is a paramount strategy to produce second-generation biofuels with high quality. In this study, polyhexamethylene biguanide hydrochloride (PHMB) is precisely added to the initial gel to synthesize nanosized ZSM-23 zeolites (Z23-*x*PH). Due to orientation adsorption and steric hindrance effects of PHMB, each sample of Z23-*x*PH demonstrates enhanced mesoporosity in comparison with the conventional Z23-C zeolite. Furthermore, the Brønsted acid density of the Z23-*x*PH samples is also significantly reduced due to a reduction in the distribution of framework Al at T2–T5 sites. The corresponding Pd/23-C and Pd/Z23-*x*PH bifunctional catalysts with 0.5 wt% Pd loading for *n*-hexadecane hydroisomerization are prepared by incorporating ZSM-23 zeolites as acid supports. According to the catalytic test results, the suitable addition of PHMB can effectively promote the *iso*-hexadecane yield. The Pd/Z23-2PH catalyst with an n_{PHMB}/n_{Si} molar ratio of 0.002 demonstrates the highest maximum *iso*-hexadecane yield of 74.1% at an *n*-hexadecane conversion of 88.3%. Therefore, the employment of PHMB has provided a simple route for the development of highly effective Pd/ZSM-23 catalysts for *n*-alkane hydroisomerization.

Keywords *n*-Hexadecane hydroisomerization · Nanosized ZSM-23 zeolite · PHMB · Bifunctional catalyst

Introduction

With the flourishing development of industrial technology in this concept of modern society, the quality demand for petrochemical products such as fuel oil and lubricating oil is gradually increasing [1–3]. Among various methods for the enhancement of fuel quality, the hydroisomerization of *n*-alkanes can effectively enhance the low-temperature fluidity of lubricating oil, increase the octane number of gasoline, and lower the freezing point of diesel [4–6]. Therefore, *n*-alkane hydroisomerization becomes the requisite process to produce second-generation biodiesel with high quality that features not only fewer olefins and aromatics but also higher energy density and enhanced miscibility with conventional diesel than first-generation biodiesel [7–9].

Metal/zeolite bifunctional catalysts have been widely applied to catalyze the hydroisomerization of *n*-alkanes and other industrial reactions [10–12]. During the reaction, *n*-alkanes generally undergo dehydrogenation at metal sites and then diffuse to Brønsted acid sites for isomerization through the cyclopropane (PCP) mechanism and eventually return to metal sites for hydrogenation to generate isomer products [13]. However, if hydrocarbon diffusion is restricted in the micropores or the Brønsted acid function is too strong, β mechanically controlled cracking reactions can occur, which can significantly lower the ideal *iso*-alkane yield [14]. Therefore, suppressing the cracking process by enhancing hydrocarbon diffusion in the microporous channels of zeolite supports or modifying the functional balance between metal and Brønsted acid sites is nonetheless remarkably pivotal for the development of bifunctional catalysts.

In addition to the improvement of metal function by employing noble metals such as Pt and Pd as metal sites, the synthesis of hierarchical zeolites with one-dimensional

✉ Wei Wang
wangw@hlju.edu.cn

✉ Wei Wu
wuwei@hlju.edu.cn

[1] National Center for International Research on Catalytic Technology, Key Laboratory of Functional Inorganic Materials Chemistry (Ministry of Education), Heilongjiang University, Harbin 150080, China

topological structures is not only remarkably precise but also a substantially systematic method to modify hydrocarbon diffusion and the metal–acid balance [15–17]. There are predominantly two strategies to synthesize hierarchical zeolites. Top-down methods that eradicate framework atoms by alkali or acid can lead to the formation of intracrystalline mesopores [18, 19]. However, alkali or acid posttreatment usually consequences in weaker hydrothermal stability of treated hierarchical zeolites and generates substantial wastewater, thereby inhibiting its further industrial applications [20, 21]. In contrast, the bottom-up strategy via the addition of mesoporous templates as growth modifiers in the initial gel to synthesize hierarchical zeolites can overcome the above disadvantages [22, 23]. For this method, the main growth modifiers are positively charged surfactants and cationic polymers that can not only adsorb on the negatively charged precursor but also restrict their further aggregation and growth [24, 25]. However, since the common growth modifiers are expensive and the crystallization condition is usually restricted, it is still crucial to discover innovative and cost-effective growth modifiers to convert the bottom-up synthesis of hierarchical zeolites more suitable for industrial applications.

Among various cationic polymers, polyhexamethylene biguanidine (PHMB) is a commercially and widely utilized spectral antibacterial agent because of its affordability, easy synthesis process, and wide upstream sources. At present, there are only a few reported works regarding the application of PHMB as the growth modifier during the synthesis of nanosized zeolites with hierarchical structure [26–28]. Su et al. [29] synthesized a series of nanosheet-assembled ZSM-5 zeolites using PHMB as the growth modifier via the microwave irradiation method, which promoted catalytic performance for the MTG reaction due to the nanosized structure formation and adjustment of Brønsted acidity. However, the employment of PHMB to synthesize nanosized zeolites for *n*-alkane hydroisomerization is still considerably determinate. Simultaneously, the influences of PHMB addition to the characteristics and catalytic performance of Pd/ZSM-23 bifunctional catalysts also require detailed investigation.

In this study, nanosized ZSM-23 zeolites are synthesized in one pot with different amounts of PHMB as a growth modifier. The Pd/ZSM-23 catalysts are further prepared for the hydroisomerization of *n*-hexadecane. The effects on the textural properties, Brønsted acidity, and catalytic performance of PHMB are analyzed.

Experimental

Materials

During the synthesis of ZSM-23 zeolite, sodium hydroxide and potassium hydroxide (both AR, Tianjin Guangfu Technology Development Co., Ltd., China) were employed to provide an alkaline environment. Aluminum sulfate octahydrate (AR, Tianjin Tianli Chemical Reagent Co., Ltd., China), pyrrolidine (PYR, AR, Shanghai Macklin Biochemical Technology Co., Ltd., China), PHMB (20%, Wuxi Jinding Longhua Chemical Co., Ltd., China), and silica sol (31.6 wt% SiO_2, Qingdao Yumin Silicone Source Reagent Factory, China) were employed as the aluminum, template, growth modifiers, and silica, respectively. A palladium nitrate solution (5 wt% Pd $(NO_3)_2$, Shaanxi Kaida Chemical Co., Ltd., China) was employed as the metal precursor for the preparation of Pd/ZSM-23 bifunctional catalysts.

Synthesis of ZSM-23 Zeolites and Preparation of Pd/ZSM-23 Catalysts

To synthesize conventional ZSM-23, the $Al_2(SO_4)_3{\cdot}18H_2O$, PYR, and silica sol were initially added to NaOH–KOH aqueous solutions with molar ratios of $Al_2(SO_4)_3/SiO_2$/PYR/NaOH/KOH/H_2O = 1:90:27:2.25:5.4:1620. The prepared initial gel was further dynamically crystallized for 48 h at 180 °C, cooled and dried at 110 °C for 12 h, and calcined at 650 °C to remove the templates. The obtained sample was then added to a 0.5 mol/L NH_4NO_3 solution at 80 °C for 8 h to get acid ZSM-23 zeolite, which was named the Z23-C sample. The nanosized ZSM-23 samples were synthesized almost the same except that PHMB was added to the initial gel and the hydrothermal crystallization time became 72 h, which were named Z23-*x*PH, where *x* was 1, 2, and 3, attributed to the addition amount of PHMB with n_{PHMB}/n_{Si} molar ratios of 0.001, 0.002, and 0.003, respectively. The Pd/ZSM-23 bifunctional catalysts were prepared by impregnating the corresponding ZSM-23 samples in a Pd $(NO_3)_2$ solution. The impregnated samples with a Pd loading of 0.5 wt% were then dried overnight at 110 °C, calcined at 600 °C for 4 h, and named Pd/Z23-C and Pd/Z23-*x*PH.

Results and Discussion

Structure and Morphology

According to the X-ray powder diffraction (XRD) patterns in Fig. 1, the diffraction peaks appear at 2θ = 8.2°, 19.7°, 22.9°, 24.7°, and 35.6° (JCPDS PDF # 37-0411) for all samples that are attributed to the MTT topological structure. Simultaneously, no peaks ascribed to other topological structures are observed, indicating that the nanosized Z23-*x*PH samples are pure. In addition to the peak positions, the diffraction intensity and calculated relative crystallinity of the Z23-*x*PH samples gradually decrease as the amount of PHMB added correspondingly increases (Table 1).

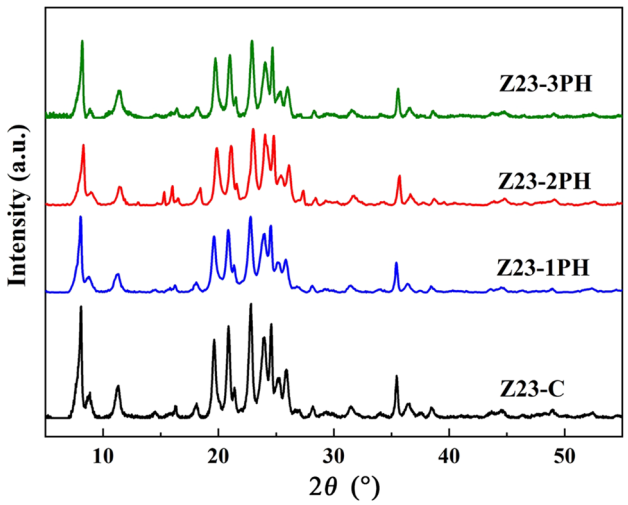

Fig. 1 XRD patterns of Z23-C and nanosized Z23-*x*PH samples

Figure 2 indicates the nitrogen physical adsorption isotherms and the BJH pore size distribution of Z23-C and Z23-*x*PH samples. The sharp rise for all ZSM-23 samples is characteristic of typical type I when P/P_0 is below 0.01, suggesting the existence of microporous saturated adsorption. Additionally, the subsequent larger hysteresis loop of the three Z23-*x*PH samples indicates the formation of more mesopores in comparison with the Z23-C sample. Furthermore, based on the BJH pore size distribution, all ZSM-23 samples exhibit mesopores ranging between 2 and 50 nm, while the peaks of the Z23-*x*PH samples are much narrower. The corresponding textural property results are displayed in Table 1. In comparison with the Z23-C sample, the microporous surface area and volume of the three Z23-*x*PH samples are all evidently reduced because of the addition of PHMB and accordingly lower relative crystallinity. In contrast, the significantly increased external surface area and mesoporous volume of the Z23-*x*PH samples demonstrate improved mesoporosity. Among all samples, the Z23-2PH sample reveals the largest mesoporosity, suggesting that a suitable amount of PHMB is pivotal for the nanosized structure formation. If the PHMB is not adequately incorporated, it is difficult to generate abundant mesopores. However, when PHMB is excessively added, the relative crystallinity may be too low to sustain the ideal textural properties.

The scanning electron microscopy (SEM) and transmission electron microscope (TEM) images shown in Figs. 3 and S1 reveal the morphologies of Z23-C and Z23-*x*PH samples. The Z23-C sample displays an aggregate morphology composed of nanosheets with a length of approximately 1.5 μm. As the amount of PHMB proliferates, the morphology of the Z23-*x*PH samples changes gradually to a spherical shape. Accounting for the employment of PHMB, the nanosheets become remarkably smaller, and the length of each crystal is below 1 μm. As a result, more intercrystalline

Table 1 Relative crystallinity and textural properties of the four ZSM-23 samples

Samples	Relative crystallinity (%)	Surface area (m^2/g)			Pore volume (cm^3/g)		
		BET[a]	Micropore[b]	External	Total[c]	Micropore[b]	Mesopore
Z23-C	100	290	211	79	0.476	0.085	0.391
Z23-1PH	87.2	281	176	105	0.617	0.073	0.544
Z23-2PH	85.4	273	166	107	0.718	0.070	0.648
Z23-3PH	79.8	232	128	104	0.591	0.054	0.537

Obtained by [a]BET method; [b]t-plot method; [c]adsorbed volume at $p/p_0 = 0.99$

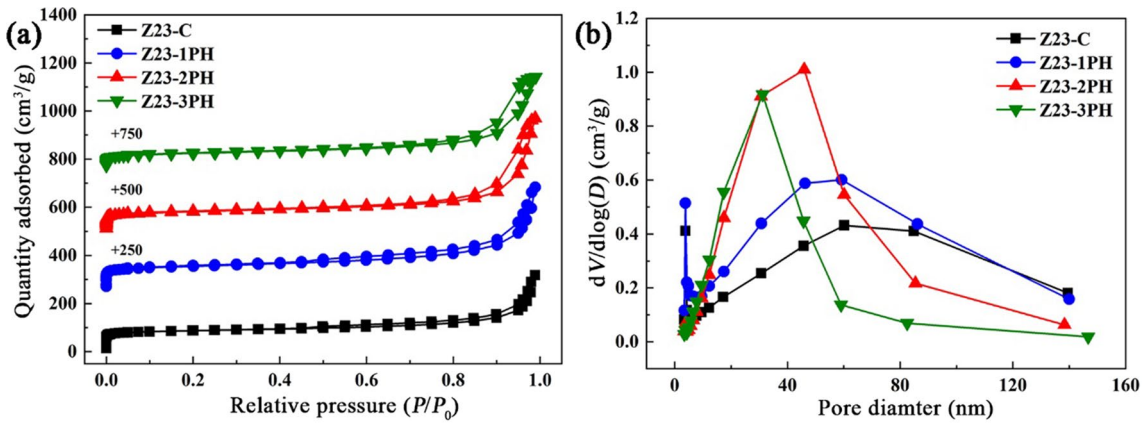

Fig. 2 **a** N_2 adsorption and desorption isotherms and **b** BJH pore size distribution of the Z23-C and Z23-*x*PH samples

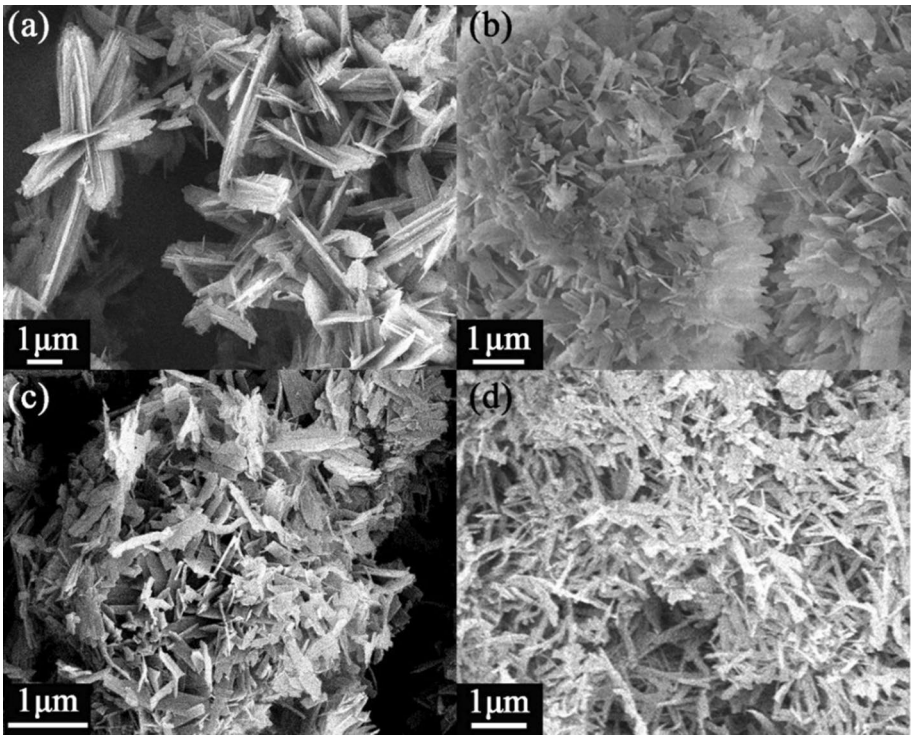

Fig. 3 SEM images of **a** Z23-C, **b** Z23-1PH, **c** Z23-2PH, and **d** Z23-3PH samples

mesopores are formed for the Z23-*x*PH samples, which is consistent with the results of N_2 physical adsorption and desorption. In order to further investigate the crystallization mechanism of Z23-*x*PH samples, ^{13}C magic angle spinning nuclear magnetic resonance spectroscopy (^{13}C MAS NMR) and thermogravimetry (TG) characterization were performed for the uncalcined Z23-C and Z23-2PH samples. According to the ^{13}C MAS NMR spectra exhibited in Fig. S2, the spectra of the Z23-C sample demonstrate strong peaks at 25.6 ppm and 47.5 ppm, which are attributed to the pyrrolidine template [30]. For the Z23-2PH sample, in addition to the peaks at 27.4 ppm and 46.7 ppm of the pyrrolidine template, new peaks associated with DAH are found at 29.6 ppm, 35.0 ppm, and 43.1 ppm, while no peaks attributed to the guanidyl species of PHMB are found at 158 ppm and 159 ppm. This phenomenon indicates that PHMB decomposes into DAH, NH_3, and CO_2 during the crystallization process, which has been encountered in our previous work [29]. Moreover, the TG curves of the Z23-C and Z23-2PH samples from 25 to 900 °C are displayed in Fig. S3. The weight loss attributed to water removal below 200 °C for Z23-C and Z23-2PH samples is 2.9% and 1.7%, respectively. In comparison, the weight loss of the organic template decomposition between 200 and 900 °C for Z23-C and Z23-2PH samples is 10.6% and 10.7%, respectively. This result indicates that the left template amounts for the two samples are almost identical. Therefore, a plausible synthesis mechanism of Z23-*x*PH samples is illustrated in scheme 1 in accordance with the above experimental results and published works. For all ZSM-23 samples, the negatively charged precursors are first generated by the depolymerization of silica and aluminum sources. Following that, unlike the crystallization process of the Z23-C sample, the additional positively charged PHMB molecules adsorbed on the negative precursor and wrapped up to impair its further growth due to the large steric hindrance. Then, the PHMB decomposes to CO_2 and NH_3 via hydrolysis under alkaline hydrothermal conditions, leading to the looser aggregation of Z23-*x*PH samples, as exhibited in the SEM images and generates more mesopores during their generation and diffusion in the crystallization process [28, 29].

Brønsted Acidity

In addition to their textural properties, the acidity of zeolite supports is another pivotal factor for hydroisomerization performance. The characterization results of the IR spectroscopy of the adsorbed pyridine (Py-IR) measurement are illustrated in Fig. S2 and Table 2. In comparison with the Z23-C sample, the Brønsted acid density of the nanosized Z23-*x*PH samples is significantly lower, which demonstrates that the application of PHMB evidently depletes the Brønsted acid density. For rationalization of this phenomenon, ^{29}Si and ^{27}Al MAS NMR measurements were further conducted for each sample of Z23-*x*PH.

Generally, the lower Brønsted acid density of zeolites originates from the reduction of bridge hydroxyl formed by framework Al atoms, which, in turn, is caused by the

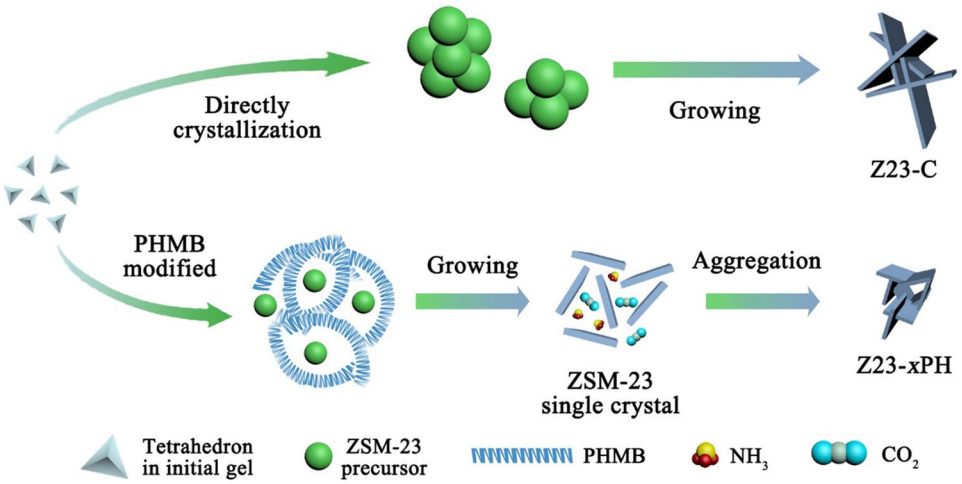

Scheme 1 The possible crystallization mechanism of the Z23-C and nanosized Z23-*x*PH samples

Table 2 Brønsted acid density with different strengths of the four ZSM-23 samples

Sample	Brønsted acid density (μmol/g)			
	Weak	Medium	Strong	Total
Z23-C	9.9	21.1	67.9	98.9
Z23-1PH	7.1	13.1	41.4	61.6
Z23-2PH	5.0	12.1	42.3	59.4
Z23-3PH	5.4	11.9	41.8	59.1

limitation of Al substitution into the framework or the distribution change of Al atoms at various framework T-sites after the PHMB addition. Therefore, the four ZSM-23 samples are first characterized by ^{29}Si MAS NMR, and the spectra are shown in Fig. S3. Via Gaussian function deconvolution integration, peaks in the ^{29}Si MAS NMR spectra for all samples are categorized into four distinct peaks at approximately − 102 ppm, − 107 ppm, − 112 ppm, and − 116 ppm, which are attributed to the chemical environments of Si(3Si1OH), Si(3Si1Al), and Si(4Si0Al), respectively [31, 32]. In accordance with their peak splitting in the ^{29}Si MAS NMR spectra, the framework Si/Al ratios are then calculated for the four ZSM-23 samples, which are listed in Table 3. It is revealed that Z23-C and Z23-*x*PH samples demonstrate similar framework Si/Al ratios, which are all above 40 and close to the inductively coupled plasma (ICP) results. This phenomenon suggests that the Al substitution in the framework of nanosized Z23-*x*PH samples is not strongly affected after the addition of PHMB.

To prove this speculation, ^{27}Al MAS NMR characterization was performed for the Z23-C and Z23-*x*PH samples, and the spectra are featured in Figs. 4 and S4. For the Z23-*x*PH samples, the strong peak appearing at approximately 56.5 ppm is ascribed to the tetrahedral coordinated Al, and the peak attributed to the nonframework Al at 0 ppm is not observed, which demonstrates that the substitution of Al atoms into the framework is not restricted and is consistent with the ^{29}Si MAS NMR results. Additionally, the ^{27}Al 2D 3Q MAS NMR spectra were recorded to obtain the quantitative proportion of Al atoms at various T-sites for the four samples (shown in Fig. S4). The chemical shift distribution is reflected by isotropic projection (F1), and the anisotropic axis (F2) contains the second-order quadrupolar line shape in the 2D plot. By deconvoluting the F1 projection spectra via the Gaussian line, the peaks attributed to the environments of Al atoms at distinct T-sites are obtained, which are summarized in Table S1 [33]. After deconvolution, five peaks are revealed around chemical shifts of 56.6 ppm, 57.3 ppm, 58.5 ppm, 59.8 ppm, and 60.3 ppm, which are

Table 3 The Si/Al ratios, relative value of Al proportion at T2–T5 sites and Brønsted acid density of the four ZSM-23 samples

Sample	Framework Si/Al ratio[a]	Bulk Si/Al ratio[b]	Proportion of Al atoms at T2–T5 sites (%)	Relative value of the proportion of Al atoms at T2–T5 sites	Relative value of total Brønsted acid density
Z23-C	44.9	42.0	60.97	1.000	1.000
Z23-1PH	42.8	41.4	37.84	0.621	0.623
Z23-2PH	46.6	43.1	35.91	0.589	0.601
Z23-3PH	43.3	41.7	37.15	0.609	0.598

[a]Calculated from ^{29}Si MAS NMR spectra;

[b]Obtained from ICP results

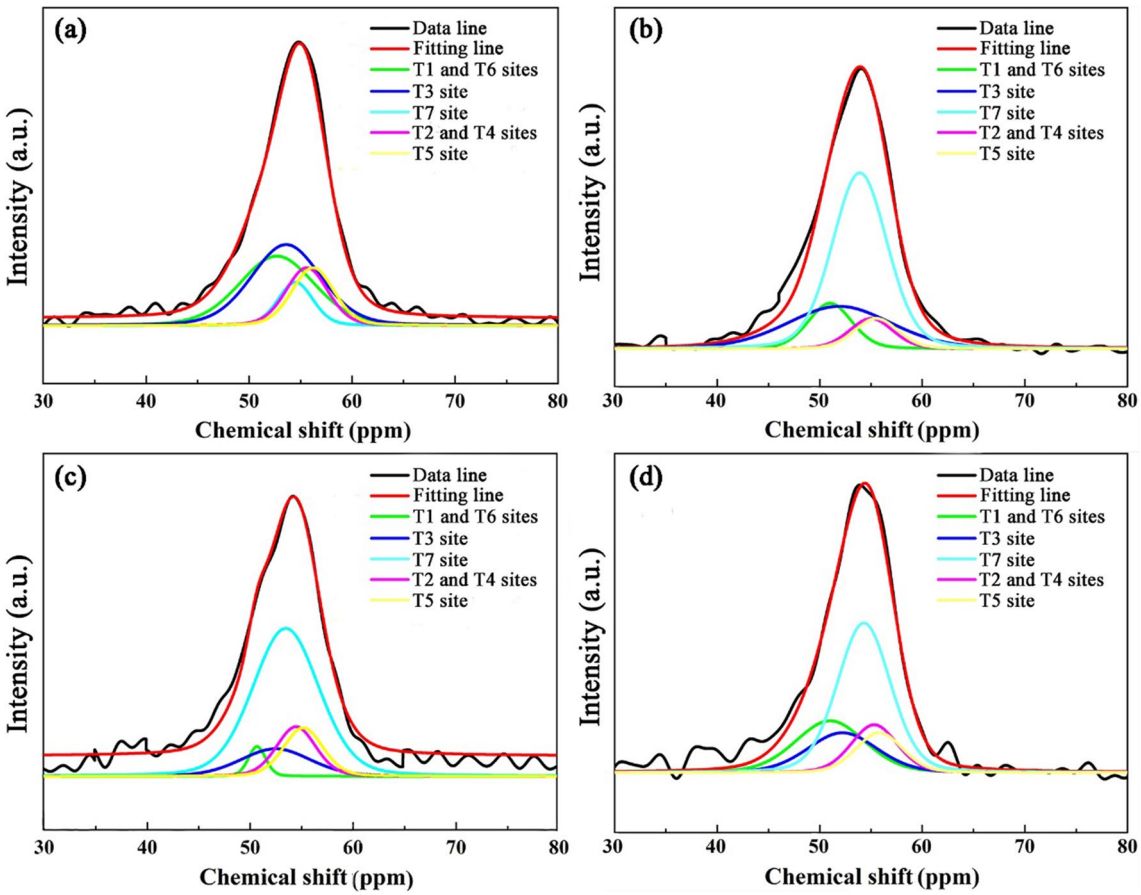

Fig. 4 ^{27}Al MAS NMR spectra of **a** Z23-C, **b** Z23-1PH, **c** Z23-2PH, and **d** Z23-3PH samples after peak deconvolution

ascribed to Al atoms at the T1 and T6, T3, T7, T2, and T4, T5 sites, respectively [34]. According to reported DFT calculation results, the T6 site in scheme S1 is at the tip of the main channel, signifying that the location of the bond angle between Al and the corresponding Si atom is almost 180° and that the bond energy is too high to keep the bond stable. Furthermore, the direct bonding between T1 and T7 Al atoms and the adjacent Si atoms at ten membered rings is also very unstable. As a result, it is considerably difficult for Al atoms located at T1, T6 and T7 to provide stable Brønsted acid sites to be detected by Py-IR measurements or catalyze the hydroisomerization [35]. Therefore, the proportion of peak areas attributed to T2–T5 sites in the ^{27}Al MAS NMR spectra demonstrates the distribution of framework Al atoms to provide detectable Brønsted acid sites. As listed in Table 3, if the proportion of T2–T5 Al atoms of the Z23-C sample is determined to be 1.000, the relative values of the corresponding proportion of the Z23-*x*PH samples are 0.621 (Z23-1PH), 0.587 (Z23-2PH) and 0.609 (Z23-3PH). Simultaneously, the relative values of the detected Brønsted acid density of the four ZSM-23 samples are also calculated. When the total Brønsted acid density of the Z23-C sample is determined to be 1.000, the relative values for the Z23-*x*PH samples are 0.622 (Z23-1PH), 0.600 (Z23-2PH), and 0.597 (Z23-3PH), which are remarkably parallel to the calculated results in accordance with the ^{27}Al MAS NMR spectra. This result indicates that the total Brønsted acid density of the ZSM-23 samples is directly affected by the distribution of T2–T5 Al atoms in the framework. Accordingly, the reduction in T2–T5 Al atoms after the addition of PHMB is the primary reason for the decline in the total Brønsted acid density for the Z23-*x*PH samples.

Characteristics of Pd/ZSM-23 Catalysts

Figure S5 and Table 4 exhibit the Py-IR characterization results of the prepared Pd/Z23-C and nanosized Pd/Z23-*x*PH bifunctional catalysts. After Pd deposition, the total Brønsted acid densities of the four Pd/ZSM-23 catalysts are all lower in comparison with the corresponding acid supports due to coverage or micropore blockage by loaded Pd nanoparticles. Furthermore, the Brønsted acid density of the four Pd/ZSM-23 catalysts declines as Pd/Z23-C > Pd/Z23-1PH > Pd/Z23-2PH > Pd/Z23-3PH.

Table 4 The characteristic of Pd/Z23-C and nanosized Pd/Z23-*x*PH catalysts

Catalyst	Brønsted acid density (μmol/g)	D_{Pd} (%)[a]	C_{Pd} (μmol/g)	C_{Pd}/C_H^+
Pd/Z23-C	76.5	34.3	16.1	0.21
Pd/Z23-1PH	45.0	32.2	15.1	0.34
Pd/Z23-2PH	44.7	32.7	15.4	0.34
Pd/Z23-3PH	44.1	35.0	16.7	0.38

[a]Data from H_2 chemisorption

Additionally, Table 4 lists the Pd dispersion obtained by H_2 chemisorption and further calculated C_{Pd}/C_H^+ values (the ratio of exposed Pd amount to total Brønsted acid density) for all Pd/ZSM-23 catalysts. The higher C_{Pd}/C_H^+ values of the Pd/Z23-*x*PH catalysts indicate a stronger metal function compared to the Pd/Z23-C catalyst, demonstrating that further isomerization or cracking caused by the stronger acid function can be effectively inhibited.

Catalytic Performance

Figure 5 presents the catalytic performance for *n*-hexadecane hydroisomerization over Pd/Z23-C and nanosized Pd/Z23-*x*PH catalysts. The *n*-hexadecane conversion results demonstrated in Fig. 5a indicate that the Pd/Z23-*x*PH catalysts illustrate enhanced catalytic activity in comparison with the Pd/Z23-C catalyst despite their lower Brønsted acid density. This phenomenon suggests that the nanosized structure is beneficial for the diffusion of hydrocarbons to active sites so that the *n*-hexadecane conversion over Pd/Z23-*x*PH catalysts is effectively enhanced. Moreover, the calculated TOF values based on Brønsted acid density also concur with this speculation. From the calculated TOF values at both 250 °C and 300 °C listed in Table 5 and Fig. S3, respectively, all Pd/Z23-*x*PH catalysts demonstrate substantially higher TOF values. This result demonstrates that all Pd/Z23-*x*PH catalysts exhibit higher catalytic activity on a single Brønsted acid site in both kinetic control and thermodynamic control regions due to enhanced diffusion of *n*-hexadecane molecules and *iso*-olefin intermediates in the channel of zeolites that is originated from enhanced mesoporosity of the Pd/Z23-*x*PH catalysts.

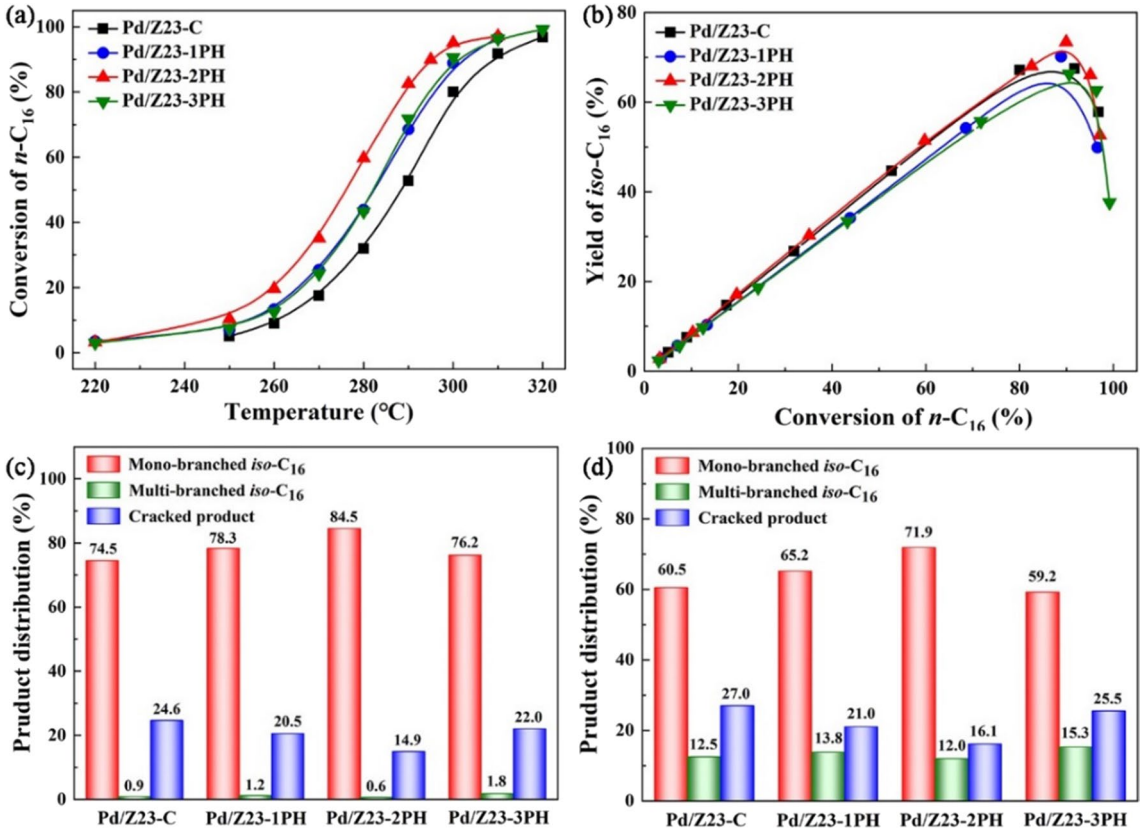

Fig. 5 The catalytic performance over the four Pd/ZSM-23 catalysts: **a** conversion of *n*-hexadecane, **b** yield of *iso*-hexadecane, products distribution at the *n*-hexadecane conversion of **c** ~ 10% and **d** ~ 90%

Table 5 The calculated TOF values at a temperature of 300 °C and n_{as} values at the *n*-hexadecane conversion of about 10% for the four Pd/ZSM-23 catalysts

Catalysts	TOF (h^{-1})	*n*-hexadecane conversion (%)	n_{as}[a]
Pd/Z23-C	168.3	9.1	1.88
Pd/Z23-1PH	339.0	13.3	1.70
Pd/Z23-2PH	350.6	10.3	1.52
Pd/Z23-3PH	325.6	12.4	1.81

[a]Detailed calculation processes are shown in Table S2

The *iso*-hexadecane yields over the four distinct catalysts are listed in Fig. 5b. Among all catalysts, the Pd/Z23-2PH catalyst demonstrates the highest *iso*-hexadecane yield of 74.1%, which is not only 7.3% higher in comparison with the Pd/Z23-C catalyst but also at a high level among the published works (Table S3). The evidently improved *iso*-hexadecane yield of the Pd/Z23-2PH catalyst originates from the higher C_{Pd}/C_H^+ value and larger mesoporosity. The higher C_{Pd}/C_H^+ values indicate a more favorable metal–acid balance, while the larger mesoporosity leads to enhanced diffusion of alkene intermediates in the acid support [36]. Accounting for these two modifications, the isomerized hexadecene intermediates can diffuse rapidly to nearby Pd sites to become *iso*-hexadecane products via hydrogenation so that further isomerization or even cracking process of isomerized hexadecane intermediates on Brønsted acid sites is effectively restrained. In addition, the n_{as} values of all catalysts are further calculated and shown in Table 5 and S3, which commonly represent the acid steps of isomer alkene intermediates taken between the dehydrogenation and hydrogenation process during the hydroisomerization. The nanosized Pd/Z23-2PH catalyst exhibits smaller n_{as} values than the Pd/Z23-C catalyst, suggesting that the acid steps occurring by hexadecene intermediates over Pd/Z23-2PH catalysts are effectively reduced, signifying that the further interaction between hexadecene intermediates and Brønsted acid sites is inhibited, and the yield of *iso*-hexadecane products is proliferated accordingly.

The product distributions over the four catalysts in Fig. 5c, d also indicate the promoted catalytic performance of the Pd/Z23-2PH catalyst. For all Pd/ZSM-23 catalysts, mono-branched *iso*-hexadecanes are the chief products despite the change in *n*-hexadecane conversion. Simultaneously, as the *n*-hexadecane conversion increases, the distribution of multibranched *iso*-hexadecane and cracking products becomes higher, indicating a stronger further isomerization and cracking process. It has been discovered that the Pd/Z23-2PH catalyst produces much higher mono-branched *iso*-hexadecane and lower cracking product proportions in comparison with the Pd/Z23-C catalyst, indicating accelerated hydrogenation of intermediates owing to the modified metal–acid balance and diffusion property. Furthermore, according to catalytic test results, the suitable addition amount of PHMB is also pivotal for the preparation of Pd/ZSM-23 catalysts with enhanced catalytic performance. When the PHMB addition is low, the modification effects of PHMB on the textural property of ZSM-23 zeolites are not adequate to retrieve evident promotion of catalytic performance. However, if PHMB is added excessively, the crystallization process of ZSM-23 crystals is severely repressed. Although the formation of a nanosized structure is beneficial for the catalytic activity of the Pd/Z23-3PH catalyst, the lower relative crystallinity results in a lower *iso*-hexadecane yield and mono-branched *iso*-hexadecane proportion in comparison with the Pd/Z23-C catalyst.

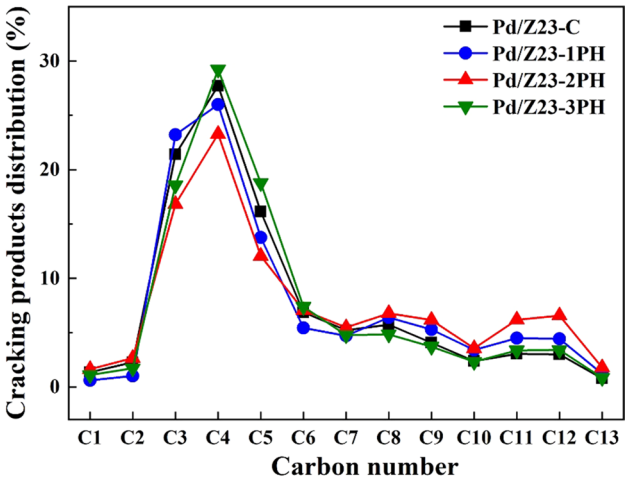

Fig. 6 Cracking products distribution over the four distinct Pd/ZSM-23 catalysts

The distribution pattern of cracking products at an *n*-hexadecane conversion of approximately 90% in Fig. 6 further indicates the influences of PHMB on the catalytic performance of Pd/Z23-*x*PH catalysts. For all Pd/ZSM-23 catalysts, a significantly strong peak is observed centered at C4, which is a typical feature of zeolite-based bifunctional catalysts [37]. This result suggests the existence of a secondary cracking process during hydroisomerization. However, the Pd/Z23-2PH catalyst demonstrates a considerably lower C4 distribution in comparison with the Pd/Z23-C catalyst, suggesting that the secondary cracking process is effectively restricted due to the modified metal–acid balance and diffusion property after the employment of PHMB.

Conclusions

In this study, nanosized Z23-*x*PH zeolites are synthesized by using PHMB as the growth modifier. The nanosized Z23-*x*PH samples demonstrate larger mesoporosity due to the

crystal growth suppression effect of PHMB attributed to its certain orientation adsorption in comparison with the Z23-C sample. Furthermore, the reduced proportion of T2–T5 Al atoms also leads to lower Brønsted acid density of Z23-*x*PH samples. Additionally, due to modified diffusion properties and metal–acid balance, the Pd/Z23-2PH catalyst with a suitable PHMB addition amount features an evidently enhanced maximum *iso*-hexadecane yield, a higher mono-branched *iso*-hexadecane proportion, and an effectively limited cracking process for *n*-hexadecane hydroisomerization. The maximum *iso*-hexadecane yield of 74.1% is retrieved at a conversion of 88.3% over the Pd/Z23-2PH catalyst, which is 7.3% higher than that of the conventional Pd/Z23-C catalyst. Therefore, the suitable PHMB addition is effective for the preparation of nanosized Pd/ZSM-23 catalysts with application potential for second-generation biodiesel production.

Supplementary Information The online version contains supplementary material available at https://doi.org/10.1007/s12209-023-00377-8.

Acknowledgements This study was funded by the National Key Research and Development Project, Intergovernmental International Science and Technology Innovation Cooperation Key Project (No. 2018YFE0108800), National Natural Science Foundation of China (No. 22278115), and Heilongjiang Province Natural Science Foundation (No. YQ2021B010).

Declarations

Conflict of interest The authors declare that there is no conflict of interest.

References

1. Fan L, Lyu YC, Fu JY et al (2023) Metal particle size effects over the Ni/SAPO-11 bifunctional catalyst. Appl Surf Sci 636:157736
2. Ding SZ, Parlett CMA, Fan XL (2022) Recent developments in multifunctional catalysts for fatty acid hydrodeoxygenation as a route towards biofuels. Mol Catal 523:111492
3. Suvarna M, Araújo TP, Pérez-Ramírez J (2022) A generalized machine learning framework to predict the space-time yield of methanol from thermocatalytic CO_2 hydrogenation. Appl Catal B 315:121530
4. Lyu YC, Yu ZM, Yang Y et al (2019) Metal and acid sites instantaneously prepared over Ni/SAPO-11 bifunctional catalyst. J Catal 374:208–216
5. Liu LL, Zhang MW, Wang L et al (2020) Construction of ordered mesopores outside MTT zeolite for efficient hydroisomerization. Appl Catal A 602:117664
6. Wang XY, Jia TH, Pan L et al (2021) Review on the relationship between liquid aerospace fuel composition and their physicochemical properties. Trans Tianjin Univ 27(2):87–109
7. Bouchy C, Hastoy G, Guillon E et al (2009) Fischer–Tropsch waxes upgrading via hydrocracking and selective hydroisomerization. Oil Gas Sci Technol Rev IFP 64(1):91–112
8. Shumeiko B, Auersvald M, Straka P et al (2020) Efficient one-stage bio-oil upgrading over sulfided catalysts. ACS Sustainable Chem Eng 8(40):15149–15167
9. Galadima A, Muraza O (2015) Hydroisomerization of sustainable feedstock in biomass-to-fuel conversion: a critical review. Int J Energy Res 39(6):741–759
10. Wang QA, Shan HC, Sim LB et al (2023) ZSM-22 synthesized using structure-directing agents of different alkyl chain lengths for controlled n-hexadecane hydroisomerizations. Ind Eng Chem Res 62(29):11470–11479
11. Jin DL, Ye GH, Zheng JW et al (2017) Hierarchical silicoaluminophosphate catalysts with enhanced hydroisomerization selectivity by directing the orientated assembly of premanufactured building blocks. ACS Catal 7(9):5887–5902
12. Lian SS, Sun KH, Wang QL et al (2023) Elucidating the roles of acid site on benzene production from methane dehydroaromatization over the supported Mo catalysts. Chem Phys Lett 825:140619
13. Wang W, Liu CJ, Wu W (2019) Bifunctional catalysts for the hydroisomerization of n-alkanes: the effects of metal–acid balance and textural structure. Catal Sci Technol 9(16):4162–4187
14. Park KC, Ihm SK (2000) Comparison of Pt/zeolite catalysts for n-hexadecane hydroisomerization. Appl Catal A 203(2):201–209
15. Zheng YF, Ding HX, Xing EH et al (2022) Promoting hydroisomerization selectivity using channel axis reduced ZSM-48 fabricated by a combined bead-milling and porogen-assisted recrystallization method. Catal Today 405–406:30–46
16. Chen YJ, Li CA, Chen XA et al (2018) Synthesis and characterization of iron-substituted ZSM-23 zeolite catalysts with highly selective hydroisomerization of n-hexadecane. Ind Eng Chem Res 57(41):13721–13730
17. Guo K, Ma AZ, Wang ZJ et al (2022) Investigation of n-heptane hydroisomerization over alkali-acid-treated hierarchical Pt/ZSM-22 zeolites. New J Chem 46(35):16752–16763
18. Liu SY, Luo CL, Deng X et al (2022) Toward rational design of narrowly-distributed mesopore on ZSM-22 zeolite for enhanced Pt dispersion and n-alkane isomerization performance. Fuel 328:125282
19. Tian QW, Liu ZH, Zhu YH et al (2016) Beyond creation of mesoporosity: the advantages of polymer-based dual-function templates for fabricating hierarchical zeolites. Adv Funct Mater 26(12):1881–1891
20. He LW, Fu WQ, Li LY et al (2021) Study of CA-treated ZSM-22 zeolite with enhanced catalytic performance in the hydroisomerization of long-chain n-dodecane. New J Chem 45(5):2820–2829
21. Li XY, Sun MH, Rooke JC et al (2013) Synthesis and applications of hierarchically porous catalysts. Chin J Catal 34(1):22–47
22. Liu SY, Ren J, Zhang HK et al (2016) Synthesis, characterization and isomerization performance of micro/mesoporous materials based on H-ZSM-22 zeolite. J Catal 335:11–23
23. Wang ZY, Wang YQ, Sun C et al (2020) Seed-assisted synthesis and catalytic performance of nano-sized ZSM-5

aggregates in a one-step crystallization process. Trans Tianjin Univ 26(4):292–304
24. Han L, Cui X, Liu X (2013) Particle size control for SAPO-11 molecular sieves. Chinese Inorg Chem 29(3):565–570
25. Chen LH, Sun MH, Wang Z et al (2020) Hierarchically structured zeolites: from design to application. Chem Rev 120(20):11194–11294
26. Liu Y, Qu W, Chang WW et al (2014) Catalytically active and hierarchically porous SAPO-11 zeolite synthesized in the presence of polyhexamethylene biguanidine. J Colloid Interface Sci 418:193–199
27. Zhang F, Liu Y, Sun Q et al (2017) Design and preparation of efficient hydroisomerization catalysts by the formation of stable SAPO-11 molecular sieve nanosheets with 10–20 nm thickness and partially blocked acidic sites. Chem Commun 53(36):4942–4945
28. Shang ZY, Chen Y, Zhang LJ et al (2022) Plate-like MFI crystal growth achieved by guanidine compounds. Inorg Chem Front 9(9):2097–2103
29. Su XF, Liu BY, Feng CQ et al (2022) Rapid and low-cost synthesis of ZSM-5 zeolite nanosheet assemblies for conversion of methanol to gasoline. Microporous Mesoporous Mater 344:112215
30. Rima D, Djamal D, Fatiha D (2018) Synthesis of high silica zeolites using a combination of pyrrolidine and tetramethylammonium as template. Mater Res Express 6(3):035017
31. Feng CQ, Su XF, Wang W et al (2021) Facile synthesis of ultrafine nanosized ZSM-5 zeolite using a hydroxyl radical initiator for enhanced catalytic performance in the MTG reaction. Microporous Mesoporous Mater 312:110780
32. Lippmaa E, Maegi M, Samoson A et al (1981) Investigation of the structure of zeolites by solid-state high-resolution silicon-29 NMR spectroscopy. J Am Chem Soc 103(17):4992–4996
33. Chen ZQ, Liu SY, Wang HH et al (2018) Synthesis and characterization of bundle-shaped ZSM-22 zeolite via the oriented fusion of nanorods and its enhanced isomerization performance. J Catal 361:177–185
34. Holzinger J, Nielsen M, Beato P et al (2019) Identification of distinct framework aluminum sites in zeolite ZSM-23: a combined computational and experimental ^{27}Al NMR study. J Phys Chem C 123(13):7831–7844
35. Liu R, Zhang JE, Sun XL et al (2014) An oniom study of the distribution of skeletal Al atoms and Brønsted acidity in ZSM-23 zeolite. J Theor Comput Chem 13(7):1450059
36. Sun JZ, Xiong SX, Lin HL et al (2023) The effects of growth modifiers on the catalytic performance of hierarchical Pd/ZSM-23 bifunctional catalysts for n-hexadecane hydroisomerization. Fuel 347:128406
37. Zhang MW, Liu LL, Wang L et al (2022) Four-carbon segmented discrete hydrocracking of long-chain paraffins in MTT channels following a pore-mouth mechanism. ACS Catal 12(16):10313–10325

Prof. Wei Wang received his PhD degree in 2016 and B.S. degree in 2011, both in Chemical Engineering from Tianjin University. He is now working at Heilongjiang University, Harbin, China. He is a board member of the Chemical Industry and Engineering Society of Heilongjiang Province, China. His scientific interests are related to the fabrication of novel nanomaterials and new catalysts for electrochemistry, hydroisomerization and energy industrial applications. He has published 20 papers in Fuel, Fuel Processing Technology, Catalysis Science & Technology, Chemical Science, Advanced Science, Nano Energy, Microporous and Mesoporous Materials and so on.

Prof. Wei Wu is the chairman of the International Joint Research Centre for Catalytic Technology and Key Laboratory of Chemical Engineering Process & Technology for High-Efficiency Conversion. She is a vice president of chemical society of Heilongjiang province of China. Her research interest is environmental friendly catalyst and catalytic technology in the field of energy and chemical industry, including preparation, structure and catalytic properties of molecular sieves and bifunctional catalysts supported metals. She has 50 patents and has published more than 100 papers in Chem. Engineer. J., Fuel, Fuel Processing Technology, Catal. Sci. Technol., Appl. Catal. A: Gen. and Micropor. Mesorpor. Mater., and so on.